



## City Research Online

### City, University of London Institutional Repository

---

**Citation:** Patel, B., Kovacevic, A., Charogiannis, A., Alam, M. N. & Schuette, M. (2021). The use of laser-induced fluorescence to measure temperature in the leakage gaps of oil-free positive displacement rotary machines. *Measurement*, 185, 110057. doi: 10.1016/j.measurement.2021.110057

This is the accepted version of the paper.

This version of the publication may differ from the final published version.

---

**Permanent repository link:** <https://openaccess.city.ac.uk/id/eprint/27841/>

**Link to published version:** <https://doi.org/10.1016/j.measurement.2021.110057>

**Copyright:** City Research Online aims to make research outputs of City, University of London available to a wider audience. Copyright and Moral Rights remain with the author(s) and/or copyright holders. URLs from City Research Online may be freely distributed and linked to.

**Reuse:** Copies of full items can be used for personal research or study, educational, or not-for-profit purposes without prior permission or charge. Provided that the authors, title and full bibliographic details are credited, a hyperlink and/or URL is given for the original metadata page and the content is not changed in any way.

---

City Research Online:

<http://openaccess.city.ac.uk/>

[publications@city.ac.uk](mailto:publications@city.ac.uk)

---

# The use of laser-induced fluorescence to measure temperature in the leakage gaps of oil-free positive displacement rotary machines

Brijeshkumar PATEL<sup>1\*</sup>, Ahmed KOVACEVIC<sup>1</sup>, Alexandros CHAROGIANNIS<sup>2</sup>, Md nahinul ALAM<sup>1</sup>, Manuel SCHÜTTE<sup>3</sup>

<sup>1</sup> City University of London, London, UK, EC1V0HB

<sup>2</sup> LavigationUK Ltd, United Kingdom

<sup>3</sup> Lavigation GmbH, Germany

**Abstract.** Positive displacement rotary machines are widely used in industry. Their efficiency is influenced by leakage through the clearance gaps between their stationary and rotating parts. Heat transfer rates between the gas and the machine parts change during the compression process, which can cause differential expansion between them and lead to deterioration of efficiency and reliability. It is necessary to understand the physics of that heat transfer in the leakage gaps.

Laser-induced fluorescence has a potential to provide visualization of the temperature field in micron size clearances. However, this technique has not been used before to measure temperatures of a gas in leakages during operation of such machines. The present study describes an assessment of the practical use of anisole-based planar laser-induced fluorescence for the study of the temperature field of leakage flows in the clearance gaps of a Roots blower. The results confirmed the feasibility of its use for this purpose.

**Keywords:** Planar Laser Induced Fluorescence, Positive Displacement Machines, Roots blower, Leakage Flows, Temperature Field, Clearance gap.

## Abbreviations

<b>Terms</b>	<b>Symbol</b>
<i>Data acquisition</i>	DAQ
<i>Intensifier relay optics</i>	IRO
<i>Laser induced fluorescence</i>	LIF
<i>Particle image velocimetry</i>	PIV
<i>Planar laser-induced fluorescence</i>	PLIF
<i>Positive displacement machines</i>	PDM
<i>Signal to noise ratio</i>	SNR
<i>Vapour delivery module</i>	VDM

## 1 Introduction

Rotary positive displacement machines (PDM) are widely used in a vast number of industrial applications. These are the devices used to move fluids, such as liquids, gases, or slurries. Such devices displace the fluid transferred by volume changes within them. Thus,

they have an expanding cavity on the suction side and a decreasing cavity on the discharge side. Gas flows into the machine as the cavity on the suction side expands and flows out of the discharge as the cavity collapses.

The Roots blower is a good representative of rotary positive displacement machines and due to its straight lobes provides an easy access for clearance visualization in operation. As shown in Figure 1(a), the Roots blower uses two figures of-eight-shaped lobe impellers mounted on parallel shafts which rotate in opposite directions to move fluid; in this case Air. When the lobe passes over the blower inlet, a finite volume of air is trapped and is carried around the chamber by the lobes. The Air is then discharged at the blower outlet. As the lobes continue to rotate, the pressure increases in the reservoir beyond the blower outlet. The rotors are synchronised by timing gears in order to maintain clearances between the impellers by and therefore no lubrication is required [1]. Precise manufacturing of these rotors enables these clearances to be very small. However, Air can still pass through them. Thus, the pressure difference between discharge and suction causes Air to flow back from the reservoir to the low-pressure regions through these clearances (see Figure 1(b)). This flow is called leakage flow.

Clearances in oil-free rotary machines are therefore critical, since a significant loss of efficiency can occur due to internal leakage [2], [3]. Shock dynamics are present in the clearances, and their nature depends on the following factors, i) the pressure ratio across the gap, ii) the gap size, iii) type of fluid, and iv) the motion of the boundary [4]. Along with the velocity field, unsteady heat transfer is also one of dominant factors which can influence leakage losses. The temperature ratio between the wall and gas temperatures could greatly affect the transonic leakage flow field, and there is a strong two-way coupling between aerodynamics and heat transfer [5]–[7]. Therefore, it is essential to study heat transfer phenomena in clearances of PDMs in order to quantify its effect on the reliability and efficiency of the machine.

In the past, experiments were carried out to visualize the flow field in the clearance gap using both Schlieren technique [8] and PIV [9]. A numerical approach to analyse the effect of the clearances on compressor performance was developed by Kovacevic [10]. An investigation of flow through the male rotor housing clearance of screw machines was carried out by Utri [11] who compared simulation results with flow pictures obtained using the Schlieren method. Recently, an experimental and numerical study of a roots blower in actual running condition was carried out by Sun et al. [12], They implemented the PIV technique for clearance flow visualization. A series of factors deteriorating the results of the PIV test were observed such as the surface flaws of the transparent window, the reflection of the surface, the jitter in the phase-locking due to uncertainties in the transmission of the synchronized gear, the accumulation of the liquid particles and the pressure fluctuations. These factors caused an increase in erroneous vectors and limited the quality of measured velocity fields.

This study focuses on the development of an optical technique to visualize the temperature field in Roots blower clearances with Air as the working fluid. An optical Roots blower was developed to provide access for visualisation of the flow inside the blower to carry out this experiments.

Small amount of a fluorescence tracer particles added in fluids have become widely accepted as the tool of choice to image heat-transfer phenomena by means of LIF [13]. The seeded tracer molecules are illuminated by an UV laser and two different colours emitted from the light are captured by a camera. Some researchers have used PLIF to study heat transfer in micro-channels as well as in multiphase flows [14], [15]. In all of these applications, this was

used to examine liquid flows. The objective of the Laser-induced fluorescence (LIF) imaging in this work was to provide two-dimensional measurements of temperature distribution in Roots blower clearances with Air. Temperature measurements obtained by this method depend on several factors such as photo physics of the seeded fluorescence tracer, the inhomogeneity of the seeded material in the flow, and the quality of visualization in a small volume. Therefore, it was necessary to check the feasibility of PLIF for this application. The investigation of the technique was carried out in collaboration with LaVision GmbH, Germany.

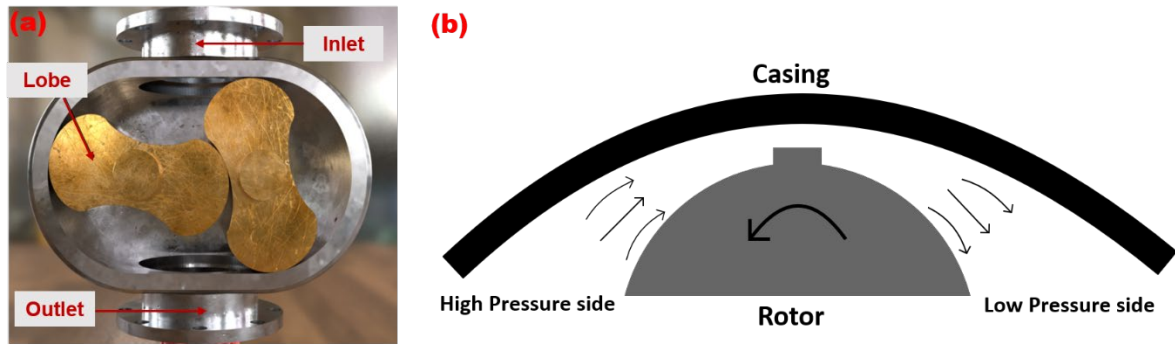


Figure 1 (a) Components of actual roots blower (b) Flow in clearance of Roots blower

## 2 Experimental analysis using PLIF method

### 2.1 Optical roots blower test rig

The schematic diagram of the Roots blower test rig is shown in Figure 2. In this study, a Howden URAI-22 oil-free Roots blower was used. The main characteristics of the used Roots blower are listed in **Table 1**. The machine is connected to a variable speed electric drive motor by a pulley transmission system to run at speeds of up to 2700 RPM. To monitor and control the operating parameters of the machine, pressure and temperature sensors were installed at suction (P1, T1), discharge (P2, T2) and at the orifice plate ( $\Delta P$ , T3) as shown in Figure 2. A shaft encoder and torque meter were used to measure the speed and power input to the Roots blower. The flow through the machine was derived from the measurements across the orifice plate. The detailed specifications of used sensors are listed in Table 2. The speed of the motor was governed by the variable frequency drive. A manually controlled ball valve, installed in the discharge line of the machine, was used to set the required discharge pressure to simulate the actual running conditions. This was limited to 2 barg, to avoid excessive discharge temperatures. All sensors were connected to a National Instrument-based data acquisition system and real-time data was recorded using LabView based programming.

It is necessary to have optical access in the machine in order to visualize the temperature field inside the Roots blower. For PLIF, the optical element should be transparent for UV light and for the present application it had to withstand temperatures and pressures of up to 300 °C and 7 barg respectively. For all these requirements, a fused silica glass is the most suitable material. As shown in Figure 3, the green highlighted portion of the casing was replaced by the fused silica glass window. Figure 4 (a) shows a complex shape of this optical glass. The optical access in radial direction where the laser sheet is applied is shown in Figure 4 (b) while the optical access to visualize the flow in the clearance gap between the rotor tip and housing is shown in Figure 4 (c). A thin gasket was provided between the metal and glass surfaces to avoid direct contact and reduce risk of the glass cracking. The glass contact was kept tight

using an external metal plate to eliminate leakage through the glass and metal mating surfaces.

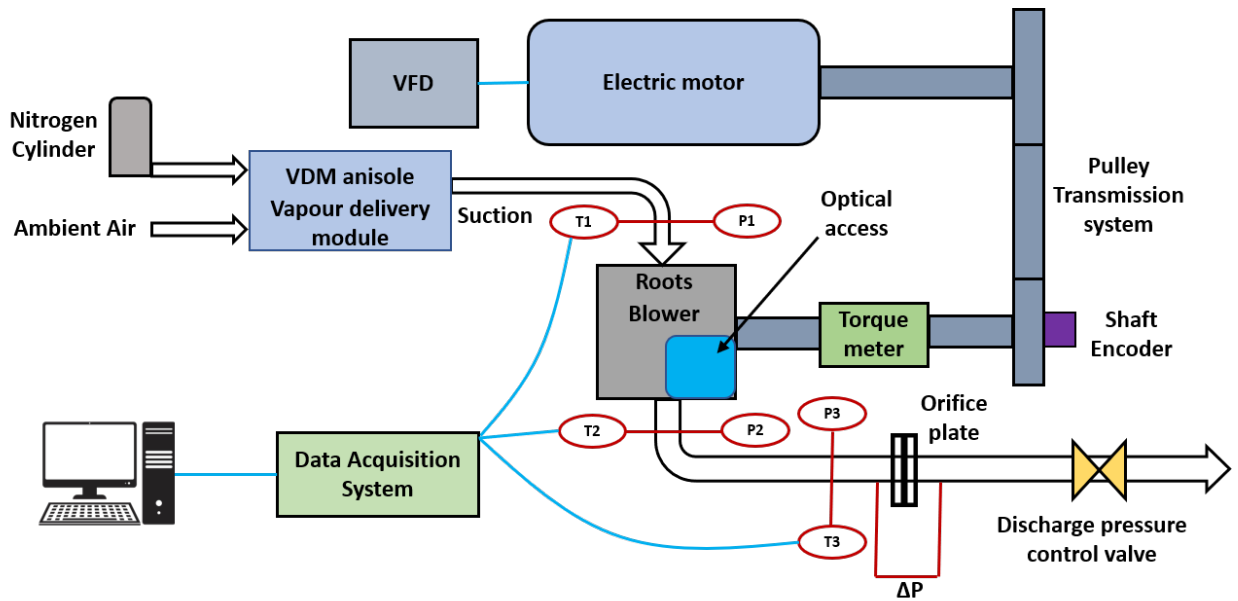


Figure 2 Schematic diagram of Roots blower test rig

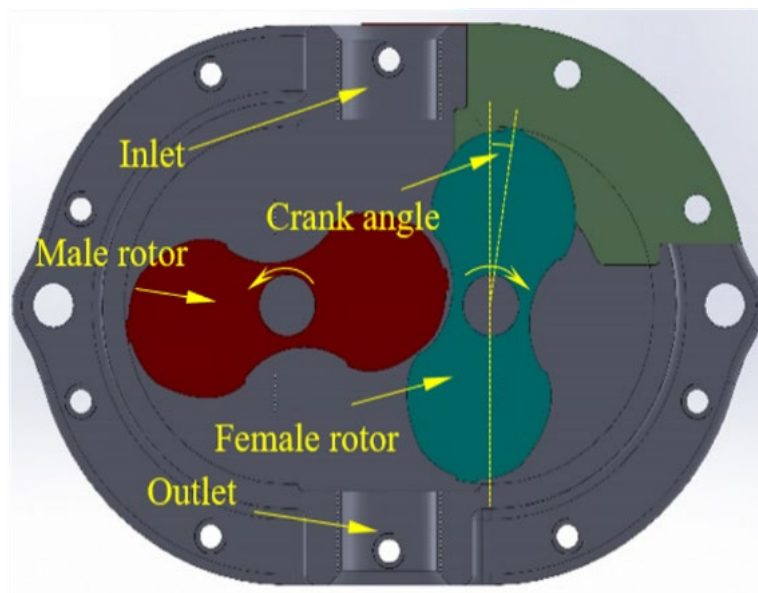


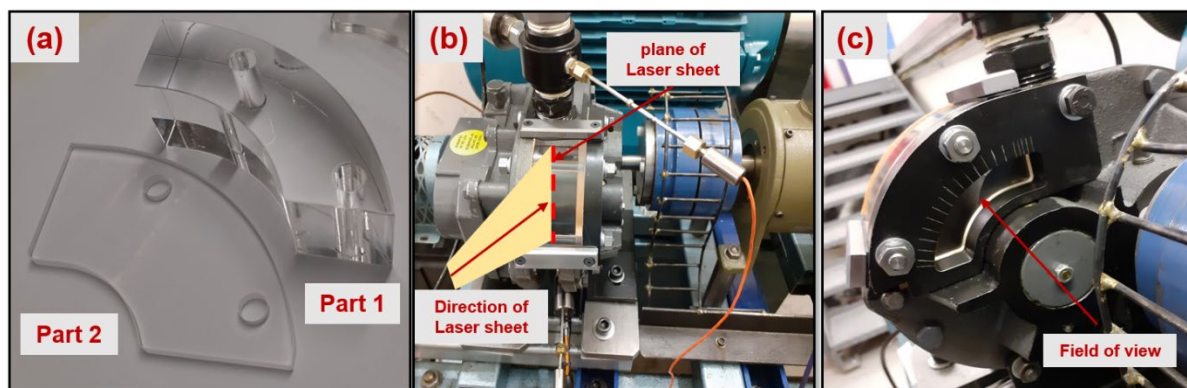
Figure 3 Rotors position in the Roots blower[9]

Table 1 The main parameters of the Roots blower

Items	Specification	Items	Specification
Diameter of the rotor [mm]	101.3	Tip gap[mm]	0.1
Axis distance [mm]	63.12	Interlobe gap[mm]	0.17
Rotor length [mm]	50.5	Axial gap[mm]	0.15
Displacement volume [l/rev]	0.4618	Width of tip step[mm]	6.4

**Table 2 Sensor specifications**

Parameters	Instrument	Specification
Speed, N	Shaft encoder (BHG 16.25W.3600-B2-5)	3600 TTL pulses per revolution Accuracy= $\pm 10\%$
Torque, T	TP-5 KMCB torque meter (strain gauge transducer)	Max capacity: 50Nm, Range = 0 - 6000 rpm, Supply volt=10v dc, Accuracy= 0.25 % of max capacity
Inlet pressure, P1	PMP5026 pressure transducer	Operating range = 3.5bar(abs) Excite voltage=12-16V dc, Output voltage = 0-10 V Accuracy = $\pm 0.2\%$ FS.
Inlet temperature, T1 Outlet temperature, T2 Orifice plate inlet Temp, T3	Platinum resistance thermometer	Range= $-75^{\circ}\text{C}$ to $250^{\circ}\text{C}$ , accuracy= $\pm 0.5^{\circ}\text{C}$
Outlet pressure, P2 Orifice plate inlet press, P3	PMP5026 pressure transducer	Operating range =15 bar (abs) Excite voltage=12-16V dc, Output voltage = 0-10 V accuracy = $\pm 0.2\%$ FS,
Orifice plate differential pressure, $\Delta P$	PMP5026 pressure transducer	Pressure diff = 0.5 bar excite voltage=12-16V dc, Output voltage = 0-10 V accuracy = $\pm 0.2\%$ FS.



**Figure 4 (a) Optical element from fused silica glass (b) Radial optical access of Roots blower to apply laser sheet (c) Optical access from side of Roots blower to visualize radial clearance**

## 2.2 PLIF Imaging

The LIF technique allows for spatiotemporally resolved, non-intrusive measurements of scalar fields, such as temperature and species concentration, by quantitatively interpreting the light emitted by a tracer molecule. Upon excitation by a light source produced from a laser, tracer molecules gain energy which is sometimes dissipated by photon emission. A camera collects these photons, and the resulting signal is quantified based on its relation to a relevant flow parameter. The quantification of this relation requires an in-depth understanding of the physics underlying the excitation process of the employed molecular tracer.

The total collected LIF signal ( $S_{LIF}$ ) can be described by the following relationship,

$$S_{LIF} = \eta_{opt} \left( \frac{E_{pulse} \lambda}{A h c} \right) V_{pix} v_{tracer} \sigma_{abs} \phi_f \quad (1)$$

Where  $\eta_{opt}$  stands for the efficiency of the collection optics and incorporates factors such as the solid angle of the detector lens and the spectral responsivity of the detection system.  $E_{pulse}$  is local laser fluence,  $h$  is Plank's constant,  $c$  is the speed of light in vacuum,  $\lambda$  is the wavelength and  $A$  is the laser sheet area. Altogether the bracketed term represents the number of excitation photons per laser-sheet cross-sectional area. The size of the imaged volume ( $V_{pix}$ ) along the laser sheet propagation times the tracer number density ( $v_{tracer}$ ) gives the number of tracer molecules available for excitation. The last two terms, the absorption cross-section ( $\sigma_{abs}$ ) and the fluorescence quantum yield ( $\phi_f$ ) account for the photophysical dependencies of the fluorescence signal and represent the probability of absorption and the efficiency of fluorescence emission respectively. The fluorescence properties of aromatic tracers such as toluene, naphthalene and anisole have been investigated, calibrated and employed in an engine-relevant planar Air-to-fuel ratio measurement as well as in thermometry studies [13]. In this study anisole is used as a tracer. The anisole tracer has strong absorption rate in the UV region and high signal sensitivity to temperature and oxygen concentration. Also, anisole yields the best signal per volume in both Nitrogen and Air. In terms of signal alone, anisole is a good choice for the compression of Air considered in this paper [16].

The two-colour detection approach (2-colour LIF) requires the illumination of the seeded volume and the subsequent detection of the emitted fluorescence by two detectors simultaneously (each looking at a different part of the emission spectrum). The resulting signal ratio (here abbreviated as  $S_{\lambda 1}/S_{\lambda 2}$ ) depends only on the absorption cross-section and the fluorescence quantum yield of the tracer at the respective wavelength ranges [17]. Dependencies such as the pulse-to-pulse energy variation and tracer density cancel out, while others such as the efficiency of the detection optics are incorporated in a constant ( $C$ ).

$$\frac{S_{\lambda 1}}{S_{\lambda 2}} = C \frac{\sigma_{abs} \phi_{f \lambda 1}}{\sigma_{abs} \phi_{f \lambda 2}} = f(T, v_{O_2}) \quad (2)$$

It should be noted that the signal ratio depends essentially on two parameters, the local temperature and the local oxygen concentration. Therefore, a reliable calibration would require for both these quantities to be known. The arrangement of the PLIF imaging equipment with the Roots blower test rig includes two different data acquisition systems (DAQ); one being used to operate and record the Roots blower test rig data and the other for PLIF imaging. A more detailed explanation of the equipment and its arrangement is presented in subsequent sections.

### 2.3 Development of the 2-colour LIF using single camera

A schematic drawing of the imaging system is shown in Figure 5. The beam from the Q-smart QSM-850 Nd: YAG laser at 1064 nm is guided through the  $2\omega/4\omega$  module to convert it into 266nm. A laser sheet is then formed by the combination of the sheet optics and the cylindrical lens of -50mm. The sheet had a thickness of about 1mm and it was placed at the central plane of the lobes of the Roots blower passing through the curved fused silica window. The average laser shot energy in the observation area was 100 mJ. The energy distributions

along and across the sheet is Gaussian. As the total fluorescence signal across the sheet is collected by the camera, the non-uniform distribution across the laser-sheet has tendency affect this distribution. But this does not affect the results because in 2-colour LIF, same laser-sheet illuminates the images taken through both wavelength filters which are divided by each other. Owing to spatial constraints, the emitted fluorescence light was rotated by 90° using a UV mirror and guided to the detection optics. Two emitted wavelengths of 320nm and 280nm were selected based on the fluorescent spectra of anisole [16]. For that reason, two filters are needed to capture two different wavelengths from emitted light. One filter of 320nm with 40nm bandwidth and another filter of 280nm with 20nm bandwidth were used. To capture identical flow field by a single camera, it is necessary to change filters alternately at each measuring condition. The machine was operated for a sufficient time to achieve steady state for measurements at each operating condition as shown in Table 3. Images are recorded at each operating condition by changing the filters alternately. The LaVision Imager M-Lite CMOS camera (pixel size:  $5.86 \times 5.86 \mu\text{m}^2$  and Number of Pixels:  $1936 \times 1216$  pixels) with LaVision intensified relay optics and UV camera lenses (LaVision,  $f = 100 \text{ mm}$ ,  $f/2.8$ ) were used to record images of the field of view. Detection limit for the camera was estimated by LaVision using their database of Anisole LIF data. For instantaneous images with approximately 200 counts (Image intensity), it was estimated that the standard deviation statistical uncertainty of  $\pm 20 \text{ K}$  exists at the temperature of 300 K and slightly larger ( $\pm 27 \text{ K}$ ) at 400 K. Phase-lock at a particular crank angle was achieved by an external triggering device with the custom signal modulation from LaVision. At each crank angle, 200 consecutive images were captured.

Following the two-colour strategy for measuring the temperature, the anisole fluorescence was seeded in the form of vapour using a Bronkhorst VDM (vapour delivery module). This VDM needs Nitrogen as a carrier gas to convert the liquid form of a seeding material into vapour. Nitrogen was supplied to VDM as a carrier gas and the flowrate of anisole and Nitrogen mixture was adjusted using a mass flow controller. The mixture produced in the seeder was introduced at the suction hose of the Roots blower. The seeder maximum capacity of co-flow of the Air or Nitrogen was 30 l/min. In this test, the Nitrogen co-flow was kept at 30 l/min, and the anisole flow of 7 l/min was maintained with 5 l/min of carrier Nitrogen flow. The amount of seeded flow was determined by checking the signal of the fluorescence particles in a recorded image at the beginning of the experiment. Measurements were carried out at the female rotor crank angle of 50° since this was the best position to obtain a clear image of the clearance area including upstream and downstream flow fields. The different test conditions at which measurements were recorded using a single camera are shown in Table 3. The discharge pressure and speed were increased by gradually closing the discharge valve and VFD drive respectively. The terminology used for the rotor position in relation to the crank angle is shown in Figure 3. A sample LIF image taken by the single camera is shown in Figure 7. These images only represent recorded intensities using two different filters. To derive temperature fields from these images, post processing of data is required, and it is further explained in Section 2.5.

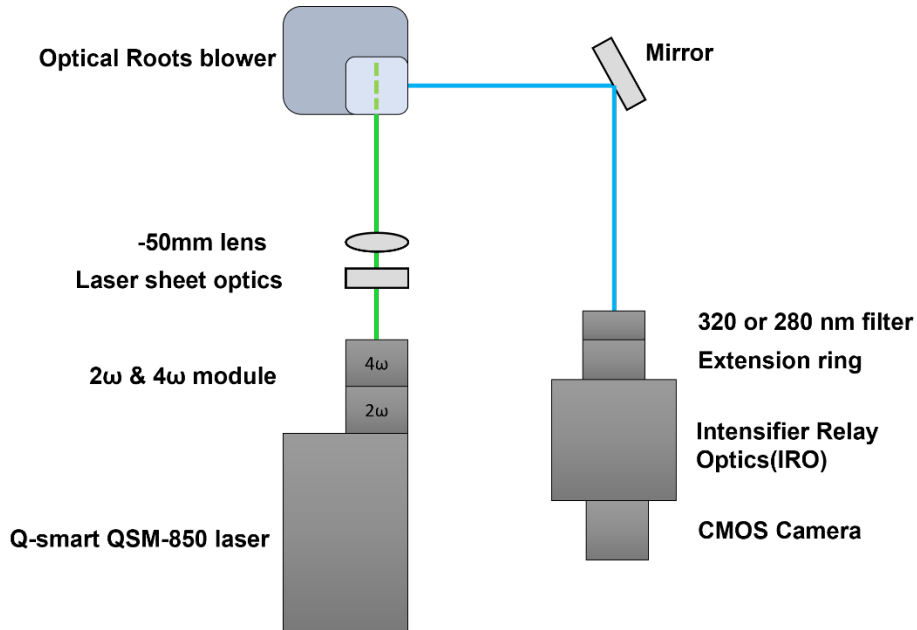


Figure 5 Arrangement of optics and Roots blower for single camera LIF imaging and measurement (a) Fused silica curved window

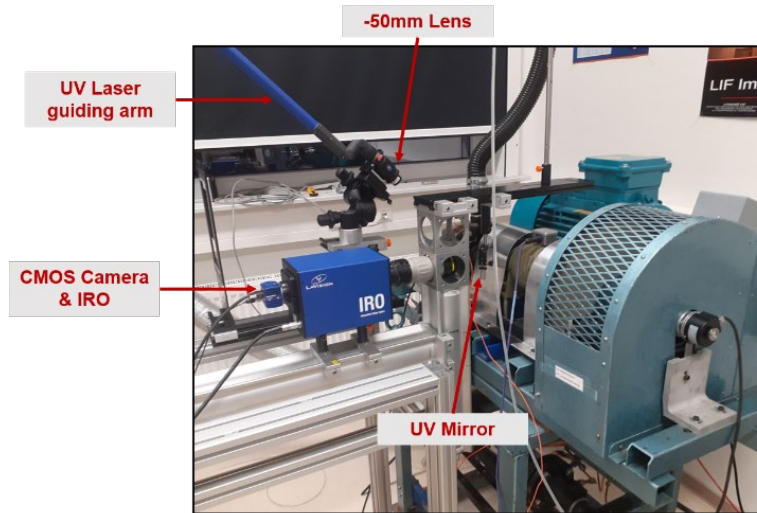
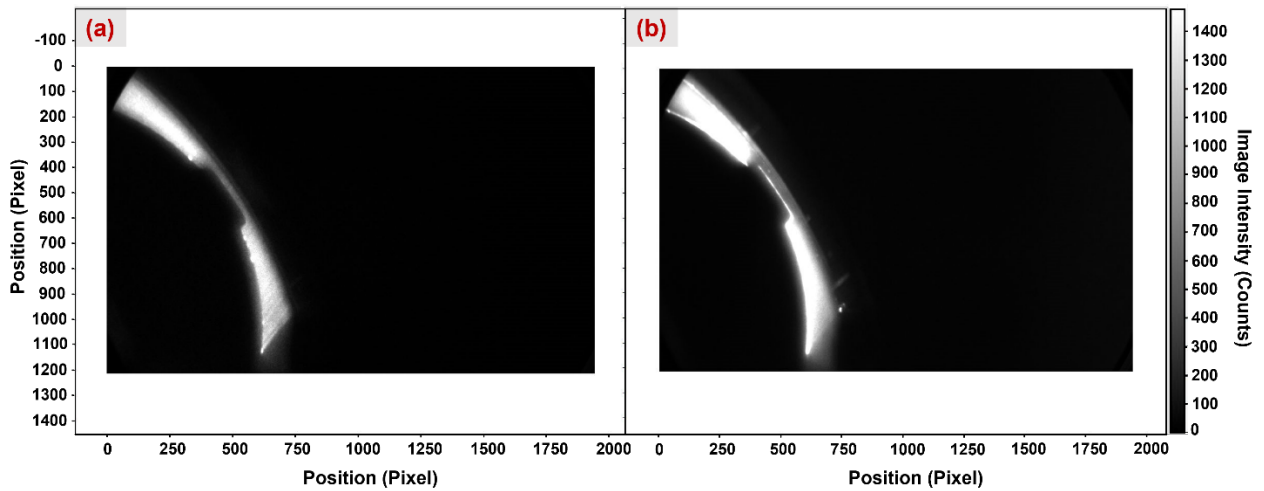


Figure 6 Single camera LIF setup

Table 3 Operating conditions during single camera LIF test

Speed (RPM)	Filter	Discharge pressure(barg)	Discharge temperature (°C)
300	320	1.04	22
	280	1.04	22
650	320	1.11	29
	280	1.11	27
900	320	1.18	37
	280	1.18	40
1200	320	1.29	59
	280	1.29	53
1500	320	1.43	80
	280	1.43	87



**Figure 7 (a) Instantaneous image at 50° crank angle captured using 320nm filter  
 (b) Instantaneous image at 50° crank angle captured using 280nm filter**

## 2.4 Development of the 2-colour LIF using two cameras

The arrangement of the equipment for two colour LIF method is similar to that of the single colour LIF, but as shown in Figure 8, the second camera was installed with an intensifier relay optics (IRO) and extension ring (32mm). Two different filters were used, 320nm and 280nm, each attached to a separate camera. The angle between the axes of the two cameras was 90° and the fluorescence spectrum was split between the two cameras using a dichroic mirror.

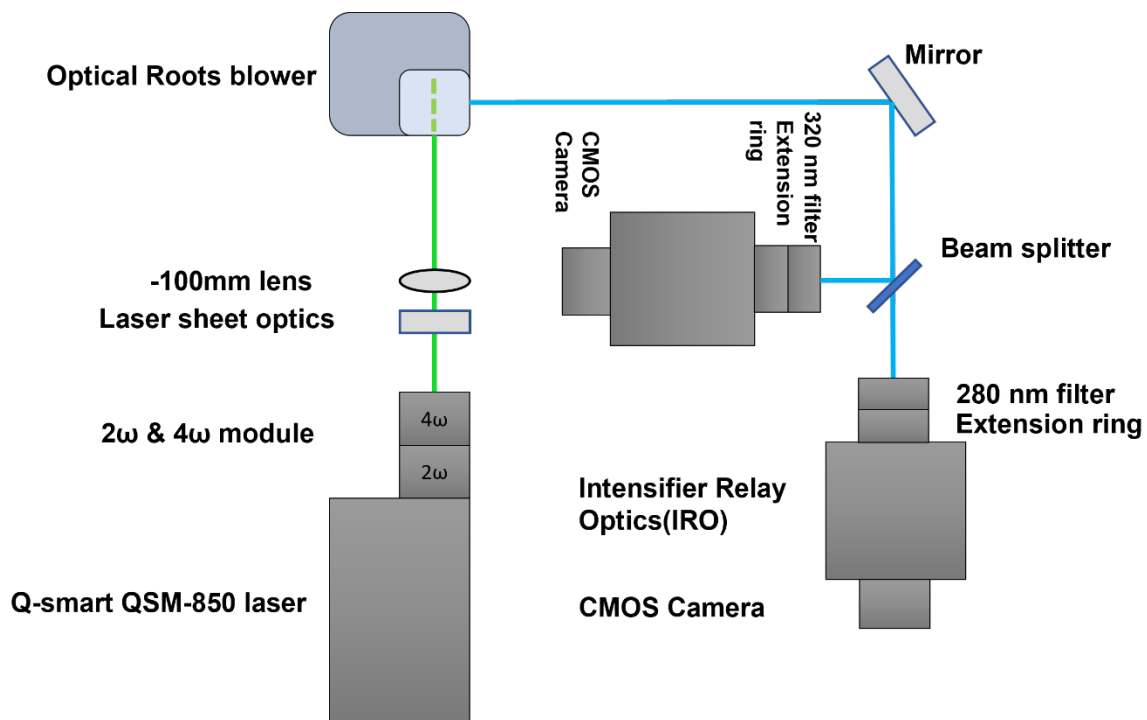


**Figure 8 Arrangement of optics and Roots blower for double camera LIF imaging and measurement**

Similarly, as for the single camera setup, a -50mm cylindrical lens was used to generate a laser sheet. The seeder allowed a supply of co-flow of Air or Nitrogen up to 30 l/min. The Air

co-flow was kept at 30 l/min, and the anisole flow of 7 l/min was maintained with 5 l/min of carrier Nitrogen flow. The Nitrogen flow was maintained to as low as possible level in order to avoid oxygen quenching but allow the seeder to operate. At the beginning of the experiment, The amount of seeded flow was determined by checking the level of fluorescence particle's signal in the recorded image. The arrangement of the two-camera LIF which enables a target field to be captured with two different filters simultaneously is shown in Figure 9. Sample frames (frame 0 and frame 1) captured by the two different cameras, when the blower was rotating at 300 RPM, are shown in Figure 10.

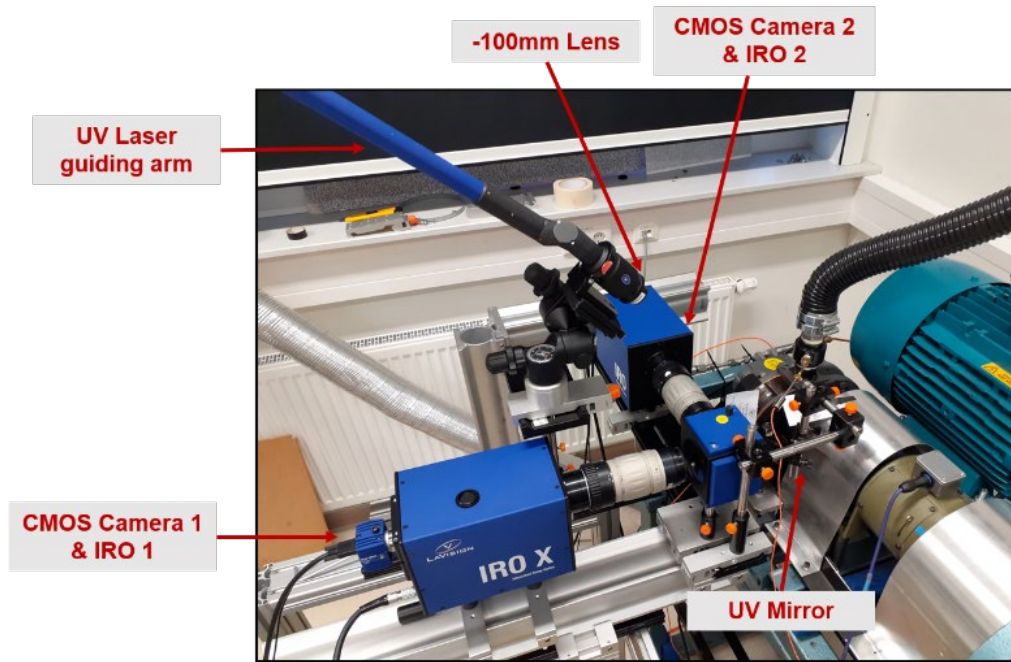


**Figure 9 Two camera LIF setup**

Different test conditions at which measurements were recorded using two cameras, are shown in Table 4.

**Table 4 Operating conditions during two camera LIF test**

Speed (RPM)	Discharge pressure(barg)	Discharge temperature (°C)
300	1.05	19
650	1.09	26
900	1.18	33
1200	1.34	44
1500	1.50	70
1800	1.65	100
2000	1.75	141

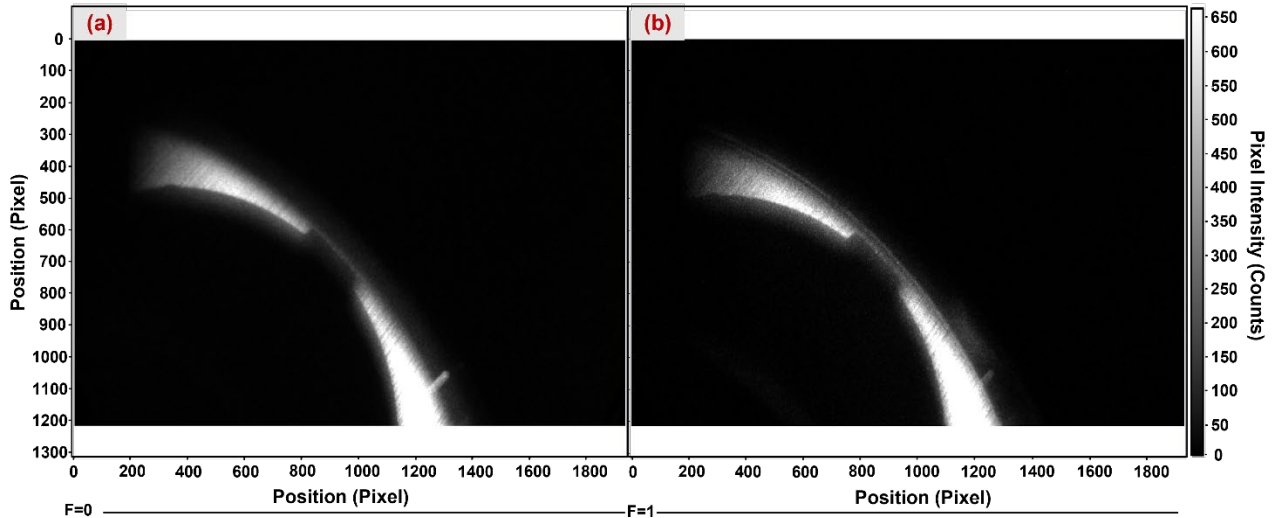


**Figure 10** Two frames captured simultaneously at 300 RPM by two camera arrangement (a) Frame 0 captured by camera using 320nm filter (b) Frame 1 captured by camera using 280nm filters

## 2.5 Temperature calibration and image processing

The biggest challenge to the development of reliable temperature calibration in the case studied in this paper was that no predefined temperature data of the flow field inside the Roots blower was available. However, it was reasonable to assume that the temperature in the large volume of the targeted field, indicated with letter V in Figure 11, was equal to the discharge temperature from the blower. This value was easily obtained from the temperature sensor in the discharge line.

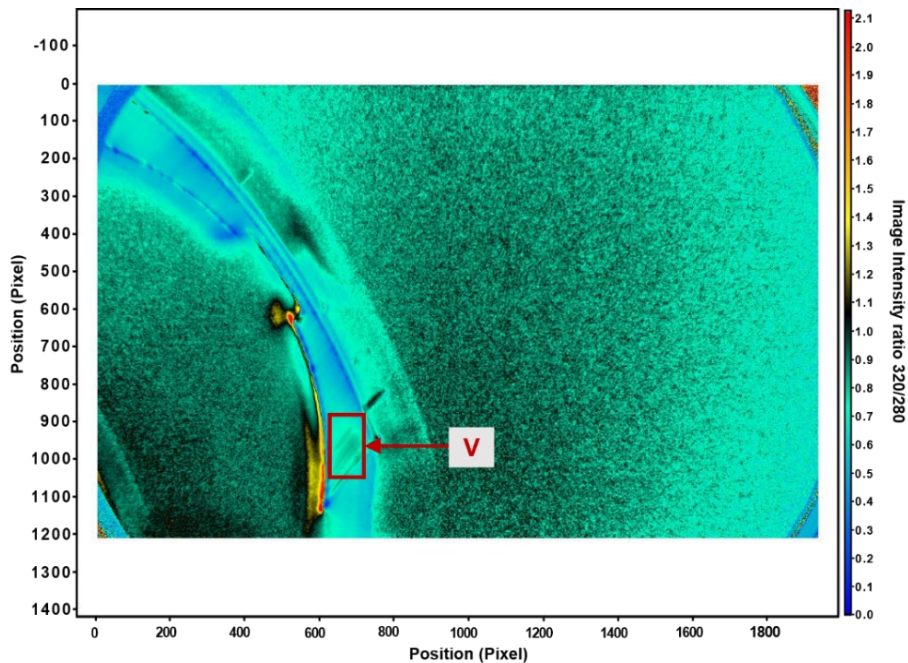


**Figure 11** Considered large volume 'V' on discharge side of the machine for temperature calibration

In order to visualize the temperature, the recorded images had to be processed. The image processing method is shown in Figure 12. According to Equation (2), the ratio of the two images can produce a temperature image. Using this principle, the 320nm image could be

divided by the 280nm image to give a temperature image. Pixel values of these image ratios are in the form of intensity. The average intensity in the large volume was mapped with the measured discharge temperature at the discharge port. This gave a correlation between the intensity and the temperature. The developed correlation was used to convert intensity values into temperature. Final images of the temperature field were generated by applying the developed correlation to all image ratios.

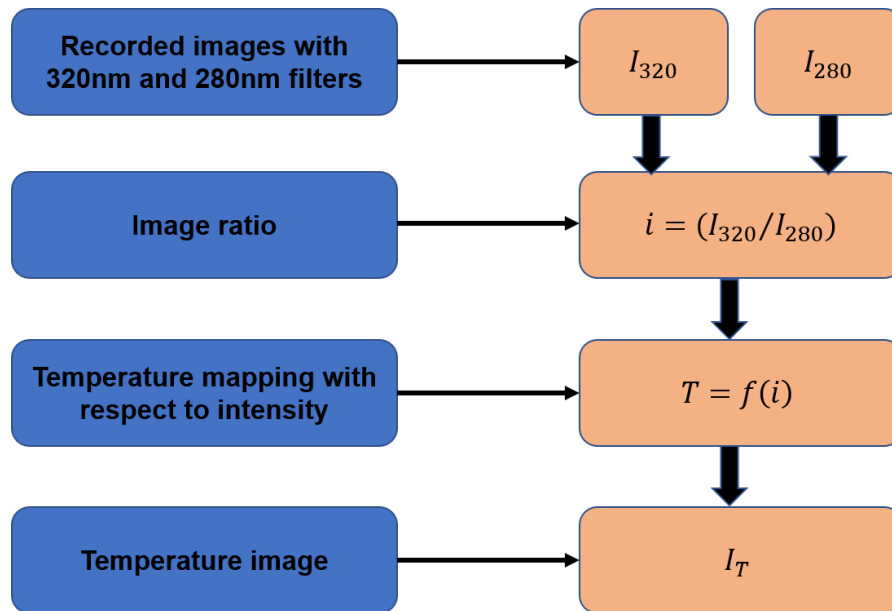


Figure 12 Schematic overview of the data processing for LIF imaging

### 3 Limitations and advantages of the developed configuration

The **single camera** procedure was required to check the quality of the temperature images to fine tune the various aspects of the study and its efficacy to analyse temperature field in the compressor clearances. However, it has a number of limitations, namely:

- i) Since time is needed to change filters for each measuring condition, the blower operating condition and hence the internal temperatures may change during this period. This may result in an incorrect estimate of temperature because the ratio of 320/280 images cannot be obtained at the same instant.
- ii) The fluorescence signal is sensitive to both temperature and oxygen concentration. The mixture of Nitrogen and anisole introduced with the Air during suction may cause oxygen quenching.
- iii) During the experiments, vaporisation of lobe paint was observed due to the high energy of the applied laser and this may be the cause of high-intensity signals from the lobe surface.

The test results for the temperature field from 300 RPM to 1500 RPM obtained by this procedure using single camera arrangement are shown in Figure 13 and Figure 14. The flow domain above section AA is the low-pressure region of the suction side while the flow domain below section AA is the high-pressure region of the discharge side. As it can be observed, with the increase in speed and discharge pressure, the bright area on the suction side increases in size and intensity (Figure 13 and Figure 14). This is most likely due to reflections

from the rotating lobe surface and glass. As speed increases, the repetition rate of the laser striking the lobe also increases. This results in the glow along the lobe and glass to extend towards the middle of the flow domain with the increase in speed. One of the options to eliminated this glow is by fine tuning the position of laser sheet. For the reason mentioned above, it is expected that temperature measurement may not be accurate in this area. Temperature variation along the section AA indicates that temperature at the centre of the clearance decreases in each case. As shown in Figure 15, the temperature curve is shifting on a higher temperature side but the temperature reduces at the centre of the clearance.

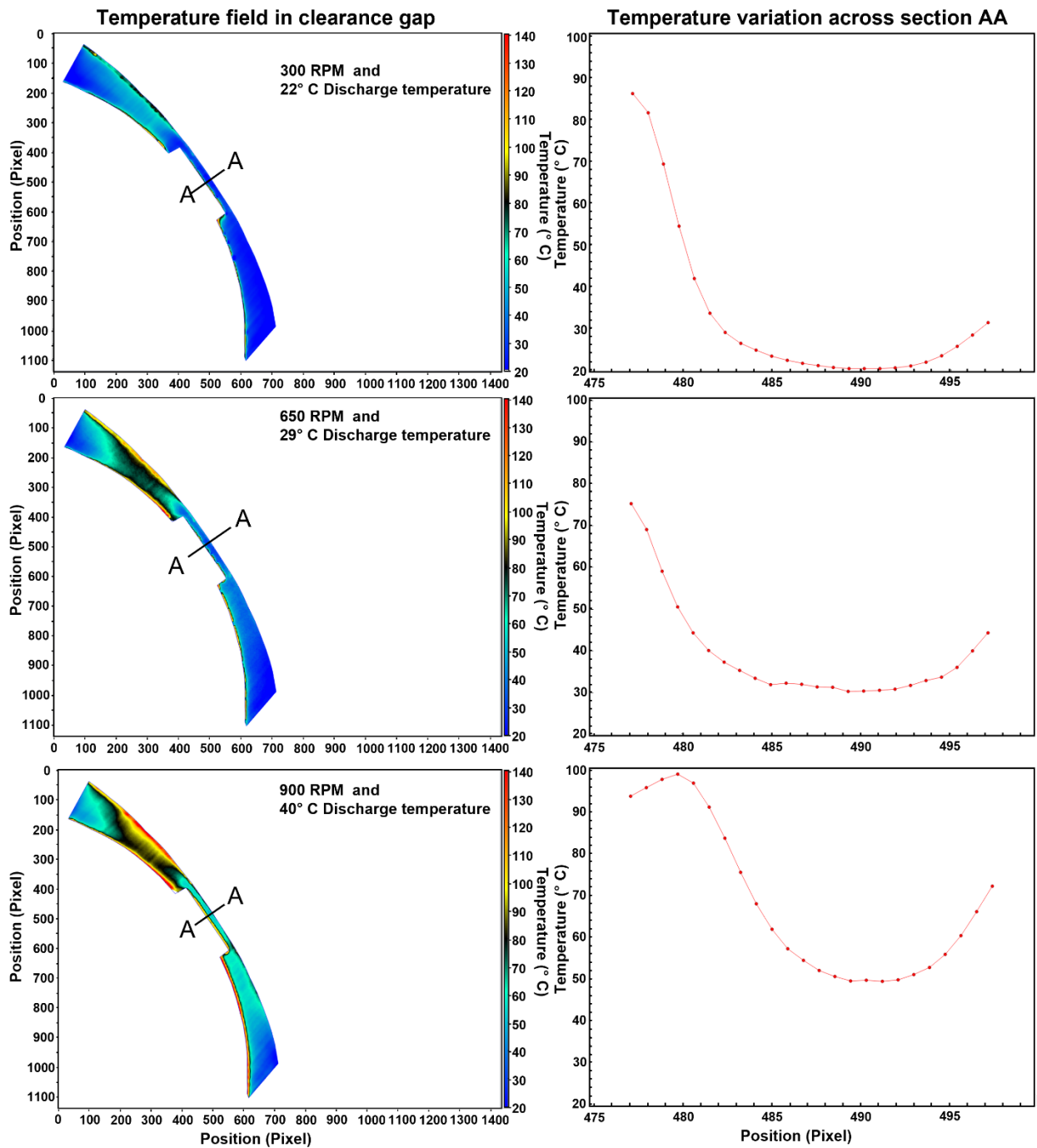


**Figure 13 Temperature field in clearance gap with temperature variation across tip clearance from single camera LIF measurement (300 to 900 RPM)**

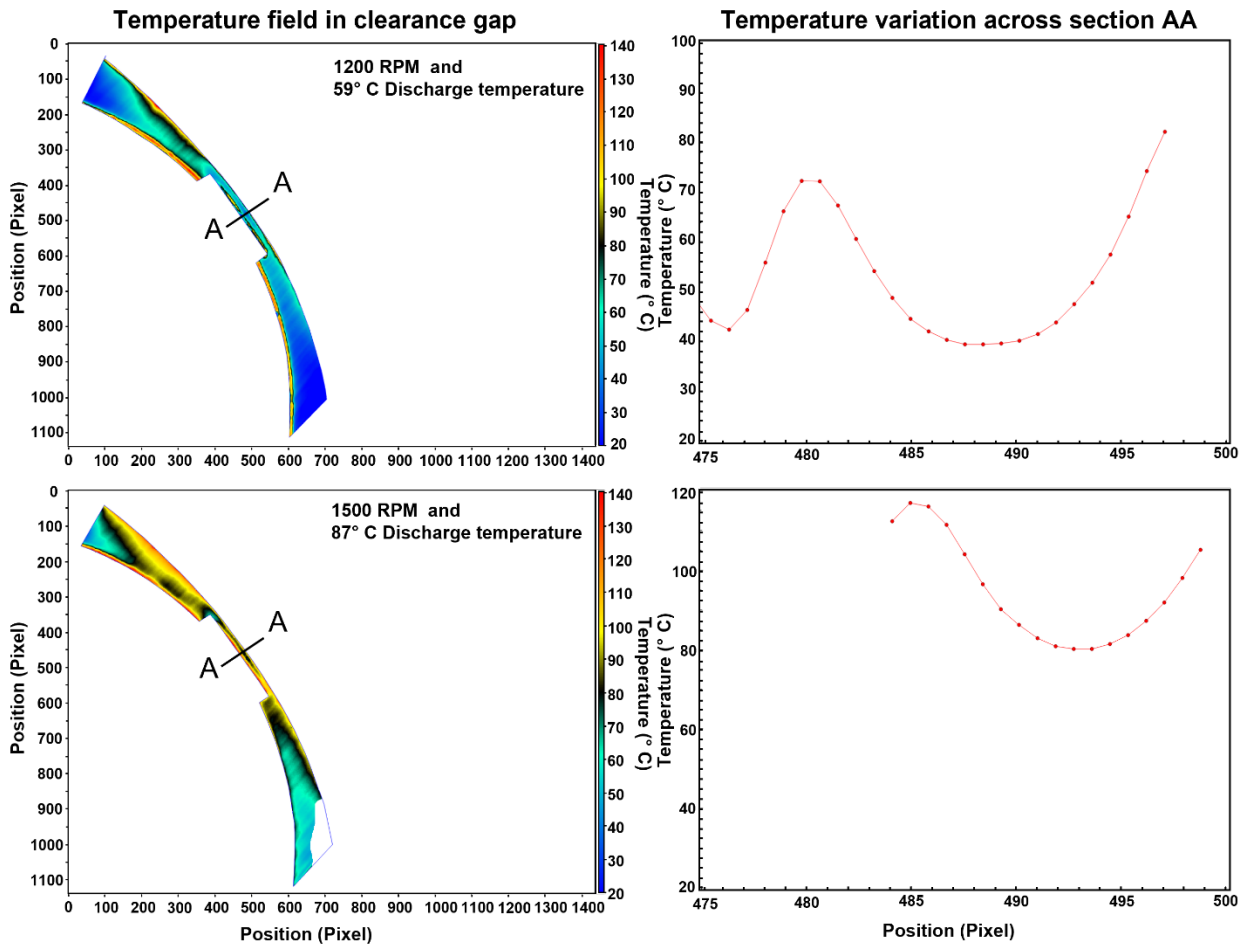


Figure 14 Temperature field in clearance gap with temperature variation across tip clearance from single camera LIF measurement (1200 & 1500 RPM)

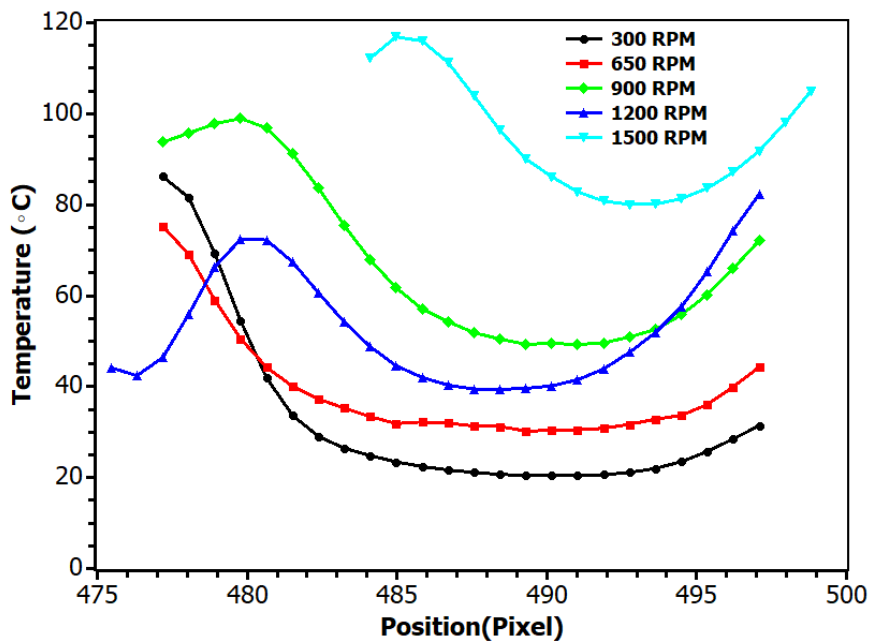
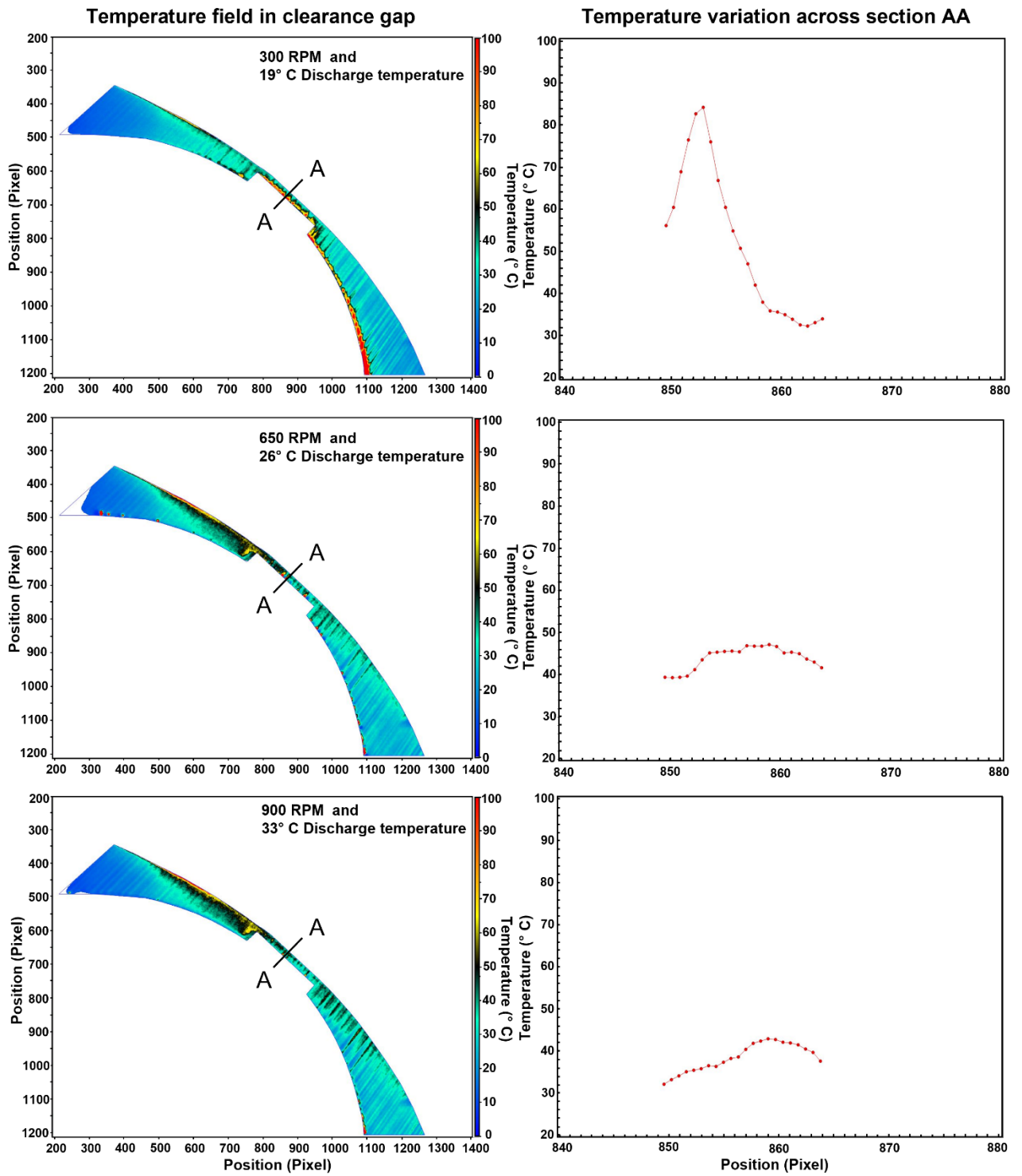


Figure 15 Comparison of temperature variation across the clearance gap at different RPM from single camera LIF measurement

**The two-camera set-up** was developed to eliminate problems encountered with the single LIF camera imaging. To eliminate the possibility of oxygen quenching, the anisole seeding line was supplied with Nitrogen while the excess Air was sucked in from the atmosphere. However, this can reduce the LIF intensity, lower signal to noise ratio and cause the need of higher IRO gain values. Oxygen quenching is the process which decreases the fluorescence intensity of an anisole. Operating the machine with pure Nitrogen could have significantly boosted the fluorescence intensity, while reducing signal to noise ratio. In addition, installing a larger focal length lens on the sheet optics could boost the collected fluorescence signal by a factor of 2 for the  $f = -100\text{mm}$  lens as it would generate less divergence along the length of the glass.

Simultaneous use of two cameras eliminated the time interval required to capture two images during single camera measurement, but introduced a problem with the image mapping since the two cameras had to be located at different locations. In other words, if one of the two cameras move then the mapping function will change and the ratio of the two images will be inconsistent at different stages of the measurement campaign. This will result in the mapping function error which is prevented using very robust mounts for cameras, intensifiers, lenses, filters and dichroic mirror. To compensate for the different locations of cameras and to generate a reliable image ratio, the image mapping was carried out in MATLAB code developed to transform the 320nm image with respect to 280nm image, using a manually calculated clearance gap and rotor tip position. The resulting temperature field thus obtained is shown in Figure 16 and Figure 17. More glares are observed in these results, and this made it difficult to visualize the temperature. As shown in Figure 18, the temperature along section AA shows randomness and has no consistent pattern. These images do not produce reliable values of temperature in the clearance gap. However, in future this issue can be resolved by implementing more reliable image mapping or by using DualScope to measure two images simultaneously with a single camera. DualScope is an optical splitting system that allows simultaneous acquisition of two spatially identical but spectrally separated images simultaneously with the use of only one single camera. Presented temperature plots are used to evaluate applicability of the PLIF technique, and the detailed error analysis along with confidence interval of quantitative results is not carried out.

Another most significant challenge associated with the two camera experiment is the generation of reliable temperature calibration for the LIF signal ratio. One approach could be to supply the Roots blower with already preheated anisole-seeded flow over a range of temperatures, operate the Roots blower in a free-flowing condition and calibrate at the desired crank angle of lobes. Alternatively, the calibration could be performed outside the Roots blower using a flow-cell; however, as the excitation arrangement and background fluorescence intensity would differ, this procedure should be carried out very carefully.



**Figure 16 Temperature field in clearance gap with temperature variation across tip clearance from two camera LIF measurement (300 RPM to 900 RPM)**

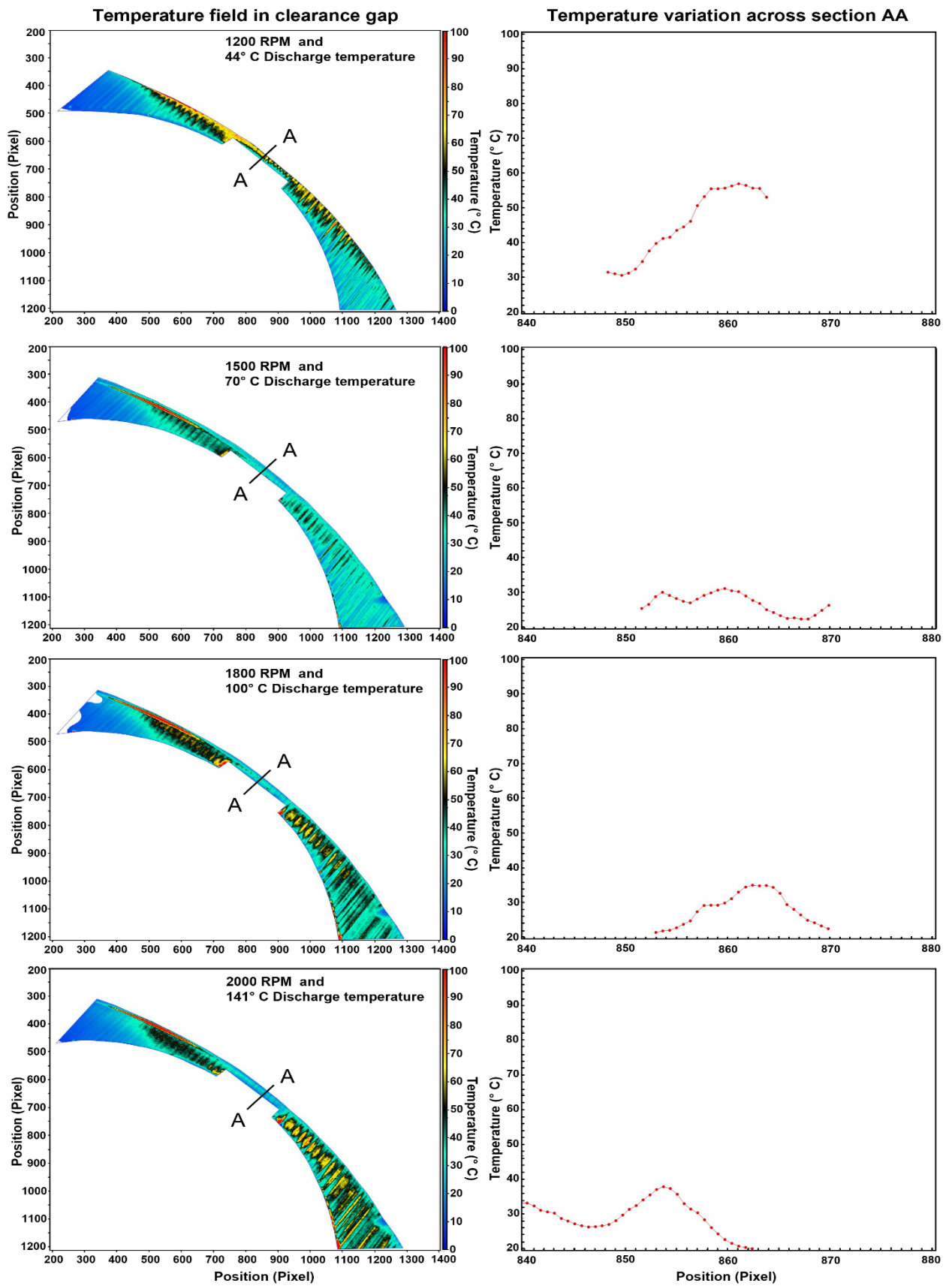


**Figure 17 Temperature field in clearance gap with temperature variation across tip clearance from two camera LIF measurement (1200 RPM to 2000 RPM)**

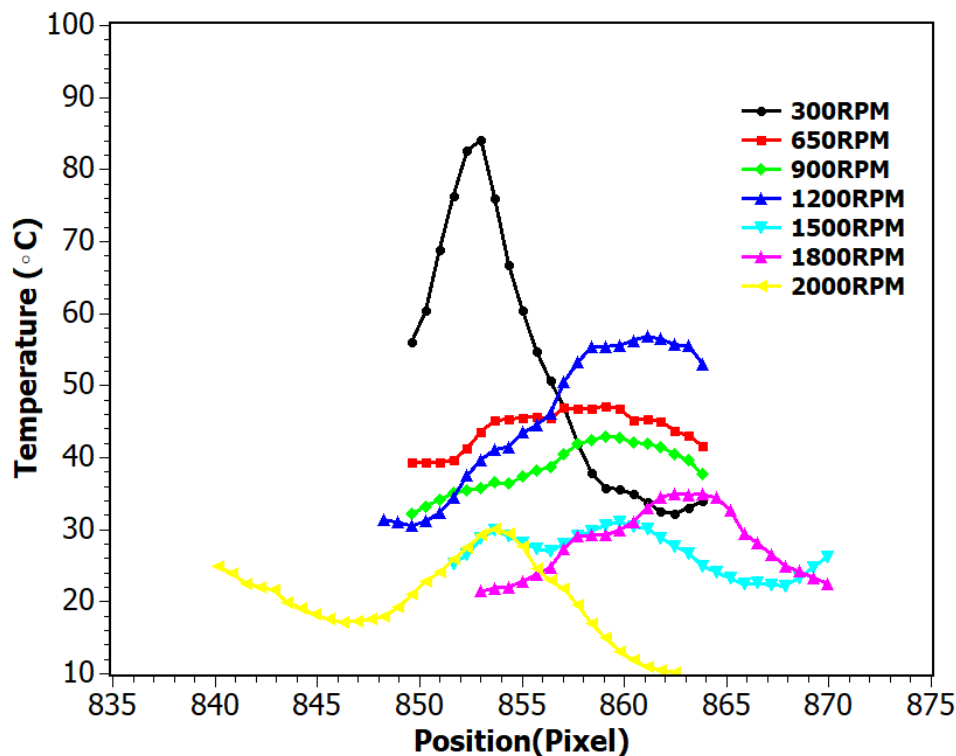


**Figure 18 Comparison of temperature variation across the clearance gap at different RPM from two camera LIF measurement**

## 4 Conclusion

An investigation of the use of anisole-based planar laser-induced fluorescence, to measure the temperature distribution in leakage flows that occur in positive displacement machines has revealed some difficulties in obtaining reliable results. Two different optical arrangements were tested for this purpose. The single-camera LIF setup does not require mapping of the two images taken with two different filter arrangements and it is easy to process the captured data. However, the use of one camera to capture two pictures, introduces errors due to the time interval required for swapping filters. A two-camera arrangement permits taking two required images simultaneously and eliminates this problem. However, two cameras cannot be located at the same position, and this creates problems in aligning the images. It was also noted that uncertainties in the initial calibration may have a significant effect on the estimated temperatures obtained from the test results. Despite these problems, it can be concluded from the obtained images that this technique has significant potential. The use of Nitrogen instead of Air as a working fluid can increase the fluorescence intensity by a factor of 5 to 10. Further work is therefore proposed and already started with an alternative camera arrangement and a calibrating procedure. It is hoped that this new research will address the uncertainties revealed by this investigation will be resolved and the new results will be reported shortly.

## 5 References

- [1] S. Mcdougald, B. W. Imrie, and B. N. Cole, "An Investigation of the Volumetric Efficiency of a Roots Blower," 1974.
- [2] J. S. Fleming and Y. Tang, "The analysis of leakage in a twin screw compressor and its application to performance improvement," *Proc. Inst. Mech. Eng. Part E J. Process Mech. Eng.*, vol. 209, no. 2, pp. 125–136, 1995.

- [3] A. M. Joshi, D. I. Blekhman, J. D. Felske, J. A. Lordi, and J. C. Mollendorf, "Clearance analysis and leakage flow CFD model of a two-lobe multi-recompression heater," *Int. J. Rotating Mach.*, vol. 2006, pp. 1–10, 2006.
- [4] P. K. Kauder and D. R. Sachs, "Gas Flow through Gaps in Screw-type Machines," 2002.
- [5] Q. Zhang and L. He, "Impact of Wall Temperature on Turbine Blade Tip Aero-Thermal Performance," *ASME 2013 Turbine Bl. Tip Symp.*, vol. 136, no. May 2014, p. V001T02A001, 2013.
- [6] H. Jiang and Q. Zhang, "Experimental evidence of temperature ratio effect on turbine blade tip heat transfer," no. c, 2018.
- [7] Q. Zhang and L. He, "Overtip choking and its implications on turbine blade-tip aerodynamic performance," *J. Propuls. Power*, vol. 27, no. 5, pp. 1008–1014, 2011.
- [8] R. Sachs, "Experimental investigation of Gas flows in screw machines," 2002.
- [9] G. Singh, S. Sun, A. Kovacevic, Q. Li, and C. Bruecker, "Transient flow analysis in a Roots blower: Experimental and numerical investigations," *Mech. Syst. Signal Process.*, vol. 134, p. 106305, 2019.
- [10] A. Kovacevic, N. Stosic, and I. K. Smith, *Screw Compressors- Three Dimensional Computational Fluid Dynamics and Solid Fluid Interaction*, vol. 53, no. 9. 2008.
- [11] M. Utri, S. Höckenkamp, and A. Brümmer, "Fluid flow through male rotor housing clearances of dry running screw machines using dimensionless numbers," *IOP Conf. Ser. Mater. Sci. Eng.*, vol. 425, p. 012033, Nov. 2018.
- [12] S. Sun, G. Singh, A. Kovacevic, and C. Bruecker, "Experimental and Numerical Investigation of Tip Leakage Flows in a Roots Blower," *Designs*, vol. 4, no. 1, p. 3, 2020.
- [13] P. Kranz *et al.*, "In-Cylinder LIF Imaging, IR-Absorption Point Measurements, and a CFD Simulation to Evaluate Mixture Formation in a CNG-Fueled Engine," *SAE Int. J. Engines*, vol. 11, no. 6, pp. 1221–1238, 2018.
- [14] M. R. Bøgild, J. L. Poulsen, E. Z. Rath, and H. Sørensen, "Investigation of heat transfer in mini channels using planar laser induced fluorescence," *J. Phys. Conf. Ser.*, vol. 395, no. 1, 2012.
- [15] A. Charogiannis and C. N. Markides, "Spatiotemporally resolved heat transfer measurements in falling liquid-films by simultaneous application of planar laser-induced fluorescence (PLIF), particle tracking velocimetry (PTV) and infrared (IR) thermography," *Exp. Therm. Fluid Sci.*, vol. 107, pp. 169–191, 2019.
- [16] S. Faust, M. Goschütz, S. A. Kaiser, T. Dreier, and C. Schulz, "A comparison of selected organic tracers for quantitative scalar imaging in the gas phase via laser-induced fluorescence," *Appl. Phys. B Lasers Opt.*, vol. 117, no. 1, pp. 183–194, 2014.
- [17] D. A. Rothamer, J. A. Snyder, R. K. Hanson, and R. R. Steeper, "Two-wavelength PLIF diagnostic for temperature and composition," *SAE Int. J. Fuels Lubr.*, vol. 1, no. 1, pp. 520–533, 2009.